

1 **Hill-based dissimilarity indices and null models for analysis of microbial**  
2 **community assembly**

3

4 Oskar Modin<sup>a\*</sup>, Raquel Liébana<sup>a</sup>, Soroush Saheb-Alam<sup>a</sup>, Britt-Marie Wilén<sup>a</sup>, Carolina Suarez<sup>b</sup>, Malte  
5 Hermansson<sup>b</sup>, Frank Persson<sup>a</sup>

6 <sup>a</sup>Water Environment Technology, Architecture and Civil Engineering, Chalmers University of Technology, Gothenburg,  
7 Sweden.

8 <sup>b</sup>Chemistry and Molecular Biology, University of Gothenburg, Sweden.

9 Email addresses: oskar.modin@chalmers.se (OM), raquel.liebana@chalmers.se (RL), soroush.sahebalam@chalmers.se (SS),  
10 britt-marie.wilen@chalmers.se (BMW), carolina.suarez@cmb.gu.se (CS), malte.hermansson@cmb.gu.se (MH),  
11 frank.persson@chalmers.se (FP)

12 \*Corresponding author

13

14 **ABSTRACT**

15

16 **Background:** High-throughput amplicon sequencing of marker genes, such as the 16S rRNA gene in  
17 Bacteria and Archaea, provides a wealth of information about the composition of microbial  
18 communities. To quantify differences between samples and draw conclusions about factors affecting  
19 community assembly, dissimilarity indices are typically used. However, results are subject to several  
20 biases and data interpretation can be challenging. The Jaccard and Bray-Curtis indices, which are  
21 often used to quantify taxonomic dissimilarity, are not necessarily the most logical choices. Instead,  
22 we argue that Hill-based indices, which make it possible to systematically investigate the impact of  
23 relative abundance on dissimilarity, should be used for robust analysis of data. In combination with a  
24 null model, mechanisms of microbial community assembly can be analyzed. Here, we also introduce a  
25 new software, qdiv, which enables rapid calculations of Hill-based dissimilarity indices in  
26 combination with null models.

27

28 **Results:** Using amplicon sequencing data from two experimental systems, aerobic granular sludge  
29 (AGS) reactors and microbial fuel cells (MFC), we show that the choice of dissimilarity index can  
30 have considerable impact on results and conclusions. High dissimilarity between replicates because of  
31 random sampling effects make incidence-based indices less suited for identifying differences between  
32 groups of samples. Determining a consensus table based on count tables generated with different  
33 bioinformatic pipelines reduced the number of low-abundant, potentially spurious amplicon sequence  
34 variants (ASVs) in the data sets, which led to lower dissimilarity between replicates. Analysis with a  
35 combination of Hill-based indices and a null model allowed us to show that different ecological  
36 mechanisms acted on different fractions of the microbial communities in the experimental systems.

37

38 **Conclusions:** Hill-based indices provide a rational framework for analysis of dissimilarity between  
39 microbial community samples. In combination with a null model, the effects of deterministic and  
40 stochastic community assembly factors on taxa of different relative abundances can be systematically  
41 investigated. Calculations of Hill-based dissimilarity indices in combination with a null model can be  
42 done in qdiv, which is freely available as a Python package (<https://github.com/omvatten/qdiv>). In  
43 qdiv, a consensus table can also be determined from several count tables generated with different  
44 bioinformatic pipelines.

45

46 **Keywords:** Aerobic granular sludge, Amplicon sequencing, Beta diversity, Bioinformatics, Microbial  
47 ecology, Microbial fuel cell

48

## 49 BACKGROUND

50 Microbial communities drive global cycles of elements and play important roles for human health,  
51 food production, and environmental engineering services such as wastewater treatment. On Earth,  
52 there may be as many as  $10^{12}$  different microbial species [1] and understanding how communities  
53 assemble, develop, and function is a formidable task. During the last decades, significant progress in  
54 DNA sequencing technology has provided a wealth of information about the diversity of microbial  
55 communities in both natural and engineered environments. Polymerase chain reaction (PCR)  
56 amplification of parts of the 16S rRNA gene followed by high-throughput sequencing using platforms  
57 such as 454 pyrosequencing, Illumina, Ion Torrent PGM, and PacBio has made it possible to probe  
58 millions of sequences in samples. For example, the Illumina MiSeq platform and dual-indexing of  
59 PCR primers allow over 100 samples to be sequenced in parallel at a depth exceeding 10 000 reads  
60 per sample [2, 3]. In addition to the rRNA gene, PCR targeting functional genes, such as the *amoA* in  
61 ammonia-oxidizing bacteria, can be used to study specific functional groups [4].

62  
63 Interpretation of results from high-throughput amplicon sequencing experiments is, however,  
64 challenging. Varying copy numbers of the target gene, sampling, DNA extraction, PCR amplification,  
65 and sequencing can all lead to biases, which distort the relative proportions of taxa in a sample [5-7].  
66 For example, Gonzalez et al. [8] showed that taxa with low abundance are typically underrepresented  
67 in PCR-based assays. PCR and sequencing also produce error-containing sequences [9]. Several  
68 computational pipelines can be used to differentiate between correct and erroneous sequence reads.  
69 After quality filtering, the reads are typically clustered into operational taxonomic units (OTUs),  
70 which are formed by grouping sequences that are similar. A similarity threshold of 97% has  
71 commonly been used. Recently, alternative approaches, which instead of OTU-clustering denoise the  
72 reads and derive exact biological sequences, have been developed [10-12]. The denoiser algorithms  
73 use different methods to differentiate between true amplicon sequence variants (ASVs) and errors.  
74 The generated ASVs can differ from each other by as little as one nucleotide, which makes it possible  
75 to investigate microbial diversity at higher resolution [e.g. 13]. Another advantage is that the ASVs  
76 represent true biological entities and can be compared to results from other sequencing runs. In OTU  
77 clustering, the centroid sequences which represent the OTUs, as well as the classification of a read to  
78 an OTU, depend on all the other sequences in the run [14]. Thus, OTU sequences do not have a  
79 meaning outside of the specific context in which they are generated [15].

80  
81 Once OTUs or ASVs have been determined, it is often of interest to study compositional differences  
82 between microbial communities in samples collected from different locations or time points (beta  
83 diversity). Indices describing the similarity or difference between sampled communities using a single  
84 number are commonly used. Many dissimilarity indices are available [16, 17]. Some, such as the  
85 Jaccard and Sørensen indices, are incidence-based, which means they do not consider differences in  
86 relative abundance between OTUs/ASVs. Other indices take the relative abundance into account. In  
87 microbial community assays it is difficult to know how much weight should be put on the relative  
88 abundance of individual OTUs/ASVs. On the one hand, we know that the read abundance and the true  
89 relative abundance of microorganisms do not always correlate in PCR-based assays [18]. Rare  
90 OTUs/ASVs often are underrepresented [8] but can play important roles for community function [19].  
91 It may therefore be tempting to use indices that weigh detected OTUs/ASVs equally. On the other  
92 hand, we know that PCR and sequencing cause errors, which may remain in the dataset after  
93 bioinformatics processing [9, 20]. Microbial communities typically also contain a long tail of  
94 extremely low-abundant taxa and random sampling affects the observed dissimilarity [5]. This view  
95 would favor the use of an index giving higher weight to abundant OTUs/ASVs; and indeed, the Bray-  
96 Curtis index, which takes relative abundance into account, is probably the most commonly used  
97 taxonomic dissimilarity index in microbial ecology (equations for the Jaccard and Bray-Curtis indices  
98 are shown in **Text S1.1, Additional file 1**). The Bray-Curtis index is very sensitive to differences in  
99 relative abundance for the most abundant OTUs/ASVs and a way to amplify the importance of

100 differences for low-abundant OTUs/ASVs is to log-transform the count data before calculating the  
 101 index [21]. However, a systematic approach for evaluating how relative abundance information affect  
 102 observed dissimilarity is lacking for the indices described above.

103

104 There are, however, other indices that deserve more attention. Hill numbers are a set of diversity  
 105 indices for which the weight given to the relative abundance of an OTU/ASV can be varied [22]. Hill  
 106 numbers, which are also called effective numbers, were originally presented as measures of alpha  
 107 diversity, i.e. OTU/ASV diversity within a community [23]. Eq. 1a-b show how Hill numbers are  
 108 calculated. The diversity order ( $q$ ) determines the weight given to the relative abundance of an  
 109 OTU/ASV in a community. For example, if  $q$  is 0, the relative abundance is not considered; if  $q$  is 1,  
 110 the OTUs/ASVs are weighted exactly according to their relative abundance; and if  $q$  is higher than 1,  
 111 more weight is given to OTUs/ASVs having high relative abundance. For a community with  $S$   
 112 OTUs/ASVs, all having the same relative abundances (i.e.  $1/S$ ), the Hill number is equal to  $S$  for all  
 113 diversity orders.

114

$$115 \quad {}^qD = \left( \sum_{i=1}^S p_i^q \right)^{1/(1-q)} \quad (\text{Eq. 1a, if } q \neq 1)$$

$$116 \quad {}^1D = \exp\left(-\sum_{i=1}^S (p_i \cdot \ln(p_i))\right) \quad (\text{Eq. 1b, if } q=1)$$

117  $D$  is the Hill number,  $q$  is the diversity order,  $S$  is the total number of OTUs/ASVs, and  $p_i$  is the  
 118 relative abundance of the  $i^{\text{th}}$  OTU/ASV in the community.

119

120 For two or more communities, Hill numbers can be decomposed into alpha ( $\alpha$ ), gamma ( $\gamma$ ), and beta  
 121 ( $\beta$ ) components [24].  ${}^qD_\alpha$  is the effective number of OTUs/ASVs per community (for a more detailed  
 122 definition, see **Text S1.2 in Additional file 1**),  ${}^qD_\gamma$  is the Hill number for the combined communities  
 123 (i.e. the regional or pooled community), and  ${}^qD_\beta$  is the ratio between the two (Eq. 2).

124

$$125 \quad {}^qD_\beta = \frac{{}^qD_\gamma}{{}^qD_\alpha} \quad (\text{Eq. 2})$$

126

127 The parameter  ${}^qD_\beta$  represents the effective number of distinct communities. It ranges from one to the  
 128 number of communities being compared ( $N$ ). If  ${}^qD_\beta=1$ , the compared communities are identical to  
 129 each other. If  ${}^qD_\beta=N$ , the compared communities are completely distinct and do not share any  
 130 OTUs/ASVs with each other.  ${}^qD_\beta$  can be transformed to an overlap or dissimilarity index constrained  
 131 between 0 and 1 (dissimilarity=1–overlap) [25]. There are several ways of doing this transformation  
 132 [26]. Chao and Chiu [27] describe two classes of overlap indices. The *local* overlap indices measure  
 133 the effective average proportion of OTUs/ASVs in a community shared with the other compared  
 134 communities. The *regional* overlap indices measure the effective proportion of OTUs/ASVs in the  
 135 pooled community that are shared between all compared communities. At a diversity order of 0,  
 136 which means only the presence/absence of OTUs/ASVs is considered, the local index equals the  
 137 Sørensen index and the regional index equals the Jaccard index. Eq. 3a-b show the transformation of  
 138  ${}^qD_\beta$  into the class of local dissimilarity indices ( ${}^q d$ ). Thus,  ${}^q d$  quantifies the effective average  
 139 proportion of OTUs/ASVs in a community *not shared* with the other compared communities.  
 140 Throughout the article, we use this local class of indices when we refer to Hill-based dissimilarity.  
 141 Further details about the calculations and equations for the class of regional indices can be found in  
 142 **Text S1.2, Additional file 1**.

143

$$144 \quad {}^q d = \frac{({}^qD_\beta)^{(1-q)} - 1}{N^{(1-q)} - 1} \quad (\text{Eq. 3a, if } q \neq 1)$$

$$145 \quad {}^1 d = \frac{\ln({}^qD_\beta)}{\ln(N)} \quad (\text{Eq. 3b, if } q=1)$$

146  ${}^q d$  is the local dissimilarity index of diversity order  $q$  and  $N$  is the number of communities being  
 147 compared.

148  
149  
150  
151  
152  
153  
154  
155  
156  
157  
158  
159  
160  
161  
162  
163  
164  
165  
166  
167  
168  
169  
170  
171  
172  
173  
174  
175  
176  
177  
178  
179  
180  
181  
182  
183  
184  
185  
186  
187  
188  
189  
190  
191  
192  
193  
194  
195  
196  
197

The use of Hill numbers is more common in the macroecological literature, both as measures of alpha diversity and for partitioning of diversity [28]. For microbial community studies using high-throughput amplicon sequencing, Hill numbers have also been recommended as measures of alpha diversity [29-31]. However, Hill-based indices are rarely used to quantify beta diversity. In two recent studies, we used Hill-based dissimilarity indices of specific diversity orders to quantify differences between microbial communities, giving different weight to the relative abundance of OTUs/ASVs [32, 33]. In this paper, we will show that examining dissimilarity ( ${}^q d$ ) for a continuum of diversity orders is a rational approach to illustrate how OTUs/ASVs with different relative abundances contribute to the dissimilarity between communities.

A difficulty with analyzing beta diversity, irrespective of the chosen index, is the interpretation of the results. We might be interested in determining if deterministic factors select for the same or different OTUs/ASVs in two sampled habitats or if the distribution of OTUs/ASVs between the habitats is governed by stochastic factors. The dissimilarity value alone tells us nothing about this. For example, if two habitats have different areas for microbial growth, the habitat with the larger area will likely have higher richness (number of detected OTUs/ASVs) because of the taxa-area relationship [34]. Since alpha- and beta diversity are not independent (Eq. 2), the richness difference will cause a high observed dissimilarity even if the two habitats select for the same OTUs/ASVs [35, 36]. Null models are useful in the interpretation of dissimilarity values and allow us to differentiate between different community assembly mechanisms [36, 37]. A null model introduced by Raup and Crick [38] and developed by Chase et al. [36] controls for richness differences between samples. Samples with pre-defined numbers of OTUs/ASVs are randomly assembled from a regional pool. The definition of the regional pool and the randomization scheme will affect the outcome of a null model analysis [39, 40]. The regional pool could consist of all OTUs/ASVs detected in the samples being compared and could also include other OTUs/ASVs that could possibly colonize the studied habitat. The randomization scheme could, e.g., be based on the frequency of samples in which a certain OTU/ASV is found [41] or the total abundance of reads associated with the OTU/ASV in the regional pool. The random assembly process is repeated many times and a null distribution for the dissimilarity between the two samples is generated. This null distribution is then compared to the observed dissimilarity. If the values are similar, the observed dissimilarity can be explained by stochastic factors. If the observed dissimilarity is higher or lower than the null expectation, there are likely deterministic factors that favor different or similar taxa in the two habitats [37]. The Raup-Crick model was originally developed for incidence-based data [36, 38] and was recently extended to also function with the Bray-Curtis index [41]. In this paper, we further extend the Raup-Crick null model to function with the whole continuum of Hill-based dissimilarity indices ( ${}^q d$ ) (**Text S1.3, Additional file 1**). The index, here denoted as the Raup-Crick index for diversity order  $q$  ( ${}^q RC$ ), is calculated using Eq. 4.

$${}^q RC = \frac{N_{[{}^q d_{exp} < {}^q d_{obs}]} + 0.5 \cdot N_{[{}^q d_{exp} = {}^q d_{obs}]}}{N_{TOT}} \quad (\text{Eq. 4})$$

$N_{[{}^q d_{exp} < {}^q d_{obs}]}$  is the number of randomizations in which the dissimilarity between the randomly assembled samples is less than between the observed samples,  $N_{[{}^q d_{exp} = {}^q d_{obs}]}$  is the number of randomizations in which the dissimilarities are equal, and  $N_{TOT}$  is the total number of randomizations.

The goal of this study is to show how the choice of dissimilarity index impact the results from high-throughput amplicon sequencing experiments. We examine sequencing data from a new experiment with aerobic granular sludge (AGS) reactors and we re-analyze a previously published data set [32] from a study with microbial fuel cells (MFCs). To reduce the effects of bioinformatics choices on the sequencing results, we examine count tables generated with several bioinformatics pipelines and use a consensus approach to infer a count table that only includes ASVs detected by two different denoiser pipelines. In the AGS experiment, we test the hypothesis that two bioreactors started from the same

198 inoculum and operated under identical conditions for 150 days exhibit the same change in microbial  
199 community composition compared to the inoculum. In the MFC experiment, we test the hypothesis  
200 that microbial communities growing in different habitats within a glucose-fed MFC are more similar  
201 than microbial communities growing in different habitats within an acetate-fed MFC. We show that  
202 the conclusions from an experiment may differ depending on the chosen dissimilarity index. We  
203 propose that a solution to this problem is to analyze community dissimilarity for a span of diversity  
204 orders using Hill-based indices, and we demonstrate that for the whole range of dissimilarity indices,  
205 null models can be used to disentangle community assembly mechanisms. Finally, we introduce a free  
206 software and Python package, qdiv, which enables rapid and simple calculations of the indices and  
207 includes an algorithm for the generation of consensus count tables. Our study focuses on taxonomic  
208 dissimilarity indices. The presented methods could, however, be extended to indices taking  
209 phylogenetic relationships into account.

210

## 211 RESULTS

212

### 213 Behavior of Hill-based dissimilarity indices and the <sup>q</sup>RC null model

214 Count tables from microbial community surveys typically consist of a few highly abundant  
215 OTUs/ASVs and many low-abundant ones. Using a highly simplified count table (**Fig. 1A-B**), we  
216 demonstrate how the Hill-based dissimilarity indices behave in comparison to the Jaccard and Bray-  
217 Curtis indices, which are more commonly used in microbial community studies. Hill-based  
218 dissimilarity (<sup>q</sup>d) are shown as functions of the diversity order, q (**Fig. 1C-D**). Since the Jaccard index  
219 is identical to the regional Hill-based dissimilarity index of diversity order 0 (**Text S1.2, Additional**  
220 **file 1**), it is plotted at q equals 0. The Bray-Curtis index is plotted at q equals 1. Bray-Curtis and Hill-  
221 based dissimilarity indices are usually not comparable. However, in the special case when two  
222 samples have the same species abundance distribution and a species detected in both samples have the  
223 exact same relative abundance in both samples, the Bray-Curtis dissimilarity is identical to <sup>1</sup>d (for  
224 proof, see **Text S1.4 in Additional file 1**).

225

226 First, let us consider the situation when samples have equal richness, i.e. the same numbers of  
227 detected species (**Fig. 1C**). Four samples (S0, S1, S2, S3) each have 2 abundant, 4 intermediate, and 8  
228 rare species. Samples S0 and S1 share 1 abundant, 2 intermediate, and 4 rare species. As expected, the  
229 Hill-based dissimilarity (<sup>q</sup>d) between S0 and S1 is 0.5 for all values of q. Sample S0 and S2 share half  
230 of the rare and intermediate species, but none of the abundant species and consequently <sup>q</sup>d goes  
231 towards 1 as q increases. Samples S0 and S3 share all intermediate species, but only 1 of the abundant  
232 and 1 of the rare, and consequently we see a valley in the <sup>q</sup>d vs q curve. In these special cases, both  
233 samples have the same species abundance distribution and a species detected in both samples have the  
234 exact same relative abundance in both samples. Consequently, the Bray-Curtis dissimilarity is  
235 identical to <sup>1</sup>d. Sample S4, however, has the same richness as S0 but a different species abundance  
236 distribution, and the Bray-Curtis index is different from <sup>1</sup>d.

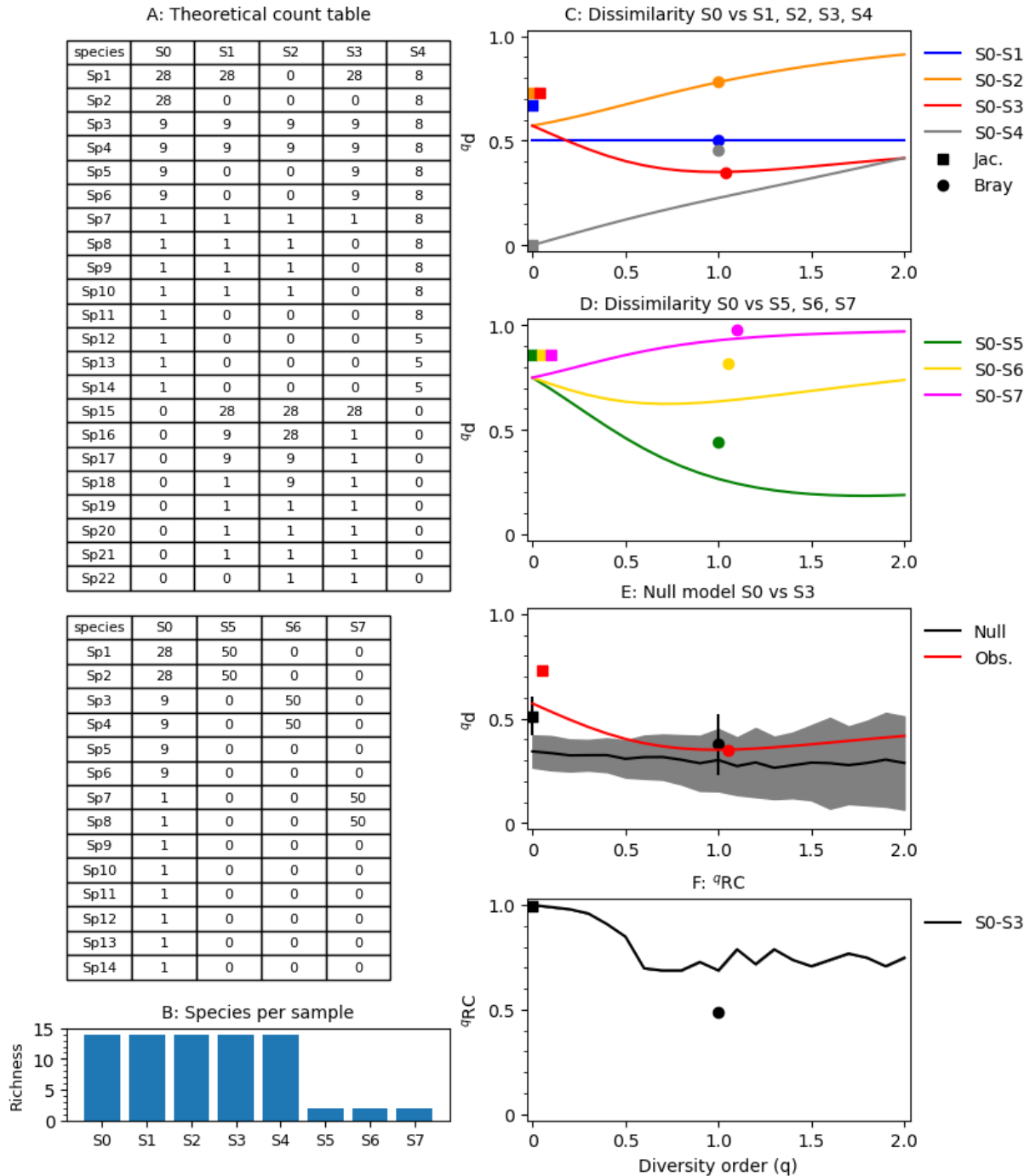
237

238 Second, let us consider the situation when samples have unequal richness (**Fig. 1D**). Samples S5-S7  
239 have only two species each. In S5, those two species are the same as the most abundant ones in  
240 sample S0 and consequently, <sup>q</sup>d decreases with increasing q. In S6, the two species are the same as  
241 two intermediates in S0 and we can see a valley in the curve. In S7, the two species are the same as  
242 two rare ones in S0 and the dissimilarity increases with q. The Bray-Curtis index shows a different  
243 behavior. For S0-S5, Bray-Curtis is equivalent to Hill-based dissimilarity with a low diversity order  
244 (q) of 0.52 and for S0-S6 and S0-S7 it is equivalent to diversity orders (q) much higher than 2.

245

246 Using the <sup>q</sup>RC null model, we can compare the observed dissimilarity between two samples to the  
247 expected dissimilarity if the two sampled communities had been randomly assembled from a regional  
248 species pool. The <sup>q</sup>RC values, as calculated in Eq. 4, are constrained between 0 and 1. A value close to

249 0 means lower dissimilarity than the null expectation and a value close to 1 means higher dissimilarity  
 250 than the null expectation. In **Fig. 1E-F**, the sample pair S0-S3 is used as an example. For values of  $q$   
 251 close to 0, the observed dissimilarity is higher than the null expectation and consequently  ${}^q\text{RC}$  is 1.  
 252 For higher values of  $q$ , the observed dissimilarity is close the null expectation and consequently the  
 253  ${}^q\text{RC}$  values are intermediate, i.e. neither close to 0 or 1 (**Fig. 1F**). For this theoretical example, it  
 254 means that if we weigh species according to their relative abundance ( $q \approx 1$ ), the observed dissimilarity  
 255 could be explained by random assembly of the two communities from the regional species pool but if  
 256 we give equal weight to all species ( $q \approx 0$ ), the observed dissimilarity is higher than we can expect  
 257 from a random assembly process.  
 258



259 **Fig. 1.** Behavior of dissimilarity indices with a theoretical data set. (A) Theoretical count table and (B) richness  
 260 of each sample. (C) Behavior of dissimilarity indices for samples with equal species abundance distribution,  
 261 sharing exactly half of the abundant, intermediate, and rare species (S0-S1), sharing no abundant but half of the  
 262

263 rare and intermediate species (S0-S2), or sharing all the intermediate species but only half of the rare and  
264 abundant (S0-S3). S0-S4 share all species but have different species abundance distributions. (D) Behavior of  
265 dissimilarity indices for samples having different richness (14 in S0 and 2 in S5-S7). In S0-S5 the shared species  
266 are the same as the most abundant in S0, in S0-S6 the shared species are those of intermediate abundance in S0,  
267 and in S0-S7 the shared species are rare in S0. (E-F) Null model analysis comparing observed dissimilarity to  
268 the null expectation for samples S0-S3. The black line and shaded region in D show the average and standard  
269 deviation for the null expectation based on 99 randomizations. Observed dissimilarity and the null expectation  
270 (E), and <sup>q</sup>RC values (F) for the Jaccard (squares) and Bray-Curtis (circles) indices are also shown.

271

## 272 **Inferring consensus count tables from the experimental data**

273 The number of low-abundant OTUs/ASVs detected when microbial communities are analyzed using  
274 high-throughput amplicon sequencing can be highly dependent on bioinformatics pipeline [42]. Here,  
275 we compare results using several pipelines operated with different settings and infer a consensus table  
276 based on the output from two denoiser pipelines. Samples collected from two experiments (AGS and  
277 MFC) were sequenced in two separate sequencing runs. The sequences were processed using  
278 DADA2 version 1.10 [43], Deblur version 1.04 [44], USEARCH version 10 [45], and Mothur version  
279 1.41 [46] with various settings, resulting in 11 count tables for each experiment. In USEARCH, we  
280 used both UNOISE to determine ASVs and UPARSE to cluster OTUs (see **Text S2.1 in Additional**  
281 **file 2**). There were large differences in the number of detected OTUs/ASVs by different pipelines.  
282 This was mostly caused by large numbers of low-abundant, potentially spurious OTUs/ASVs  
283 appearing when the pipelines were run with relaxed quality filtering thresholds. Despite the large  
284 richness differences, count tables generated with different pipelines generally had similar abundance-  
285 based diversity values and evenness. They also showed similar beta diversity patterns and were able  
286 to distinguish between different sample categories in the data sets (see **Text S2.3-4 in Additional file**  
287 **2**).

288

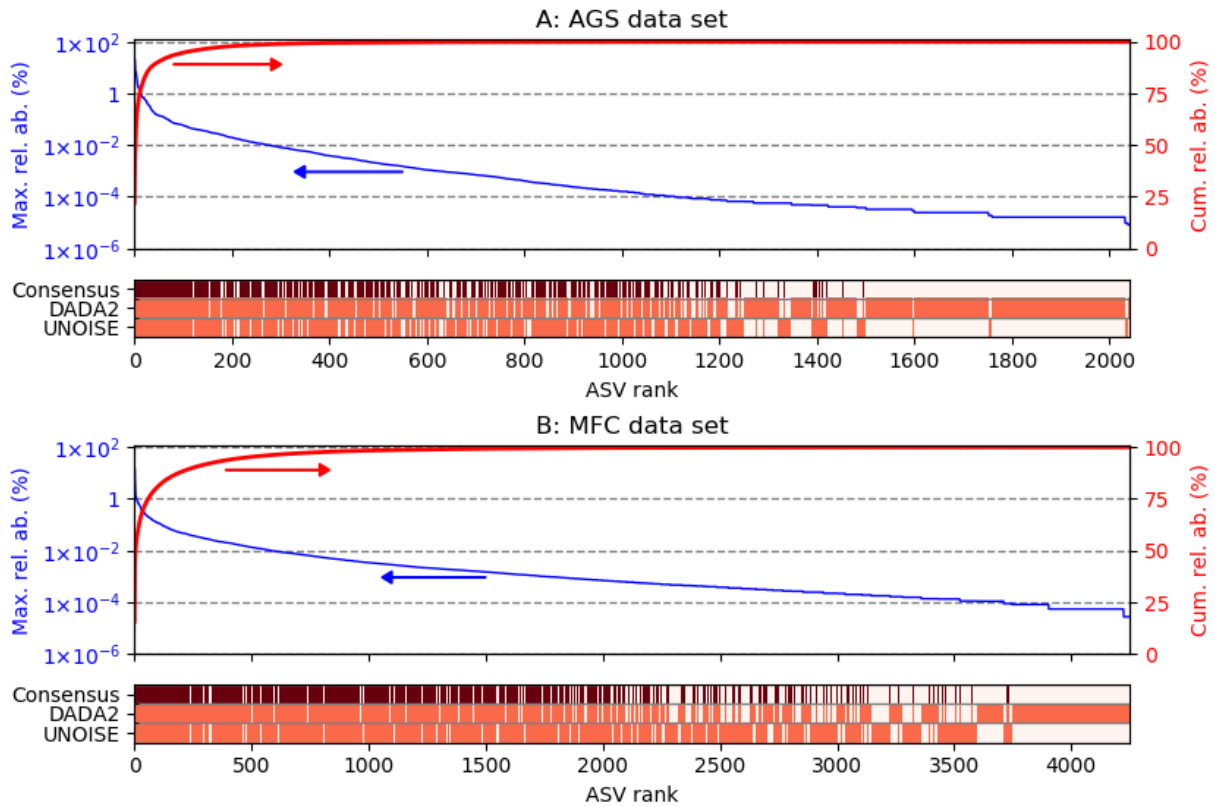
289 Denoiser pipelines generate exact ASVs, which represent true biological entities. Thus, an ASV found  
290 with one denoiser pipeline should also be found with another. To filter out potentially spurious ASVs,  
291 information from several pipelines can be combined in a consensus table. A function for generating a  
292 consensus table from an unlimited number of count tables was implemented in qdiv. The consensus  
293 function identifies ASVs that are detected in all compared count tables. For each count table, the  
294 fraction of the reads associated with the set of shared ASVs is calculated. The count table with the  
295 highest fraction is retained, all ASVs not belonging to the shared set are discarded, and the retained  
296 count table with the remaining shared ASVs is returned as the consensus table (for a more detailed  
297 description, see **Text S2.2 in Additional file 2**). In this study, we inferred a consensus table based on  
298 two count tables generated with DADA2 and UNOISE. For the AGS data set, the DADA2 and  
299 UNOISE count tables had 1768 and 1192 ASVs, respectively. The consensus function identified 919  
300 shared ASVs. The UNOISE count table had 99.7% of its read counts mapped to these shared ASVs  
301 and was retained as the consensus table after being subsetted to the shared ASVs. For the MFC data  
302 set, the DADA2 and UNOISE count tables had 3355 and 3152 ASVs, respectively. The consensus  
303 table was based on the UNOISE table, which had 99.4% of its reads mapped to the 2258 shared  
304 ASVs. The relative abundances of the ASVs detected by the count tables are shown in **Fig. 2**. The  
305 ASVs that are not retained in the consensus table have low relative abundance spanning from  $8 \cdot 10^{-6}$  to  
306  $0.05\%$  in the AGS data set and  $3 \cdot 10^{-6}$ - $0.8\%$  in the MFC data set. Before analysis of dissimilarity, the  
307 count tables were rarefied to the number of reads in the smallest sample. This was 278 758  
308 reads/sample in the AGS data set and 33 171 reads/sample in the MFC data set. Further details about  
309 the count tables are shown in **Fig. S2.1-10 in Additional file 2**.

310

311 The consensus count tables were used to evaluate dissimilarity between replicate samples and test  
312 hypotheses on the experimental data from the AGS and MFC systems.

313

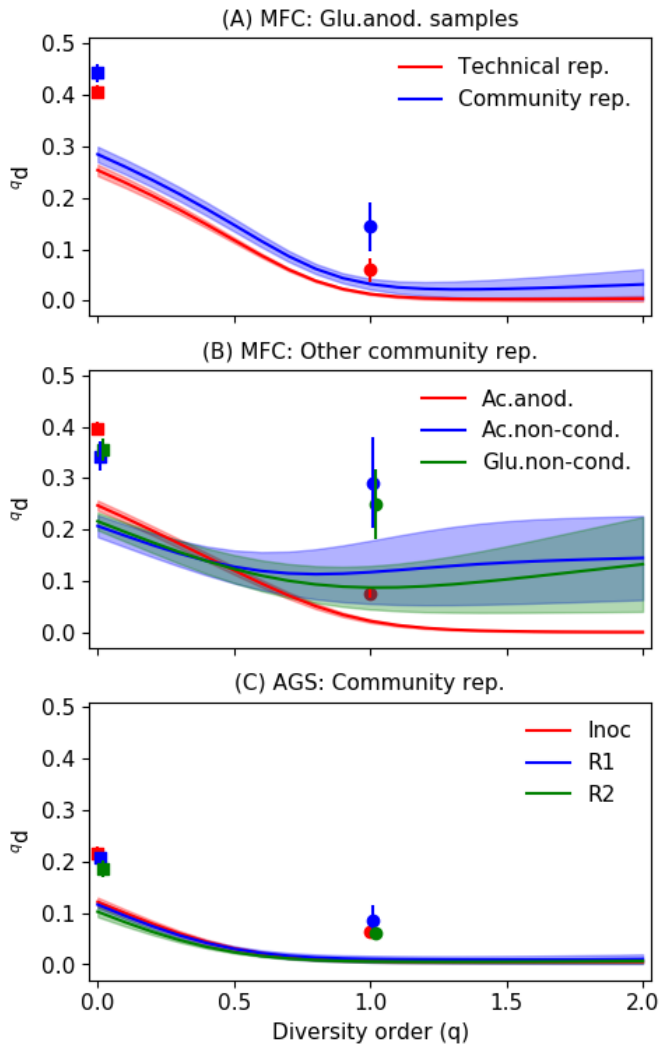




314  
 315 **Fig. 2.** Relative abundance (%) of ASVs retained in the consensus tables for the AGS (A) and MFC (B) data  
 316 sets. Each ASV in the two input tables, arranged from highest to lowest relative abundance, is shown on the x-  
 317 axis. The blue lines show the maximum relative abundances of the ASVs in the DADA2 and UNOISE count  
 318 tables and the red lines show the cumulative relative abundances. The heatmaps show whether the ASVs were  
 319 detected in the DADA2 and UNOISE count tables (light red). If it was detected in both, it was also retained in  
 320 the consensus table, which is indicated by dark red color.

321  
 322 **The observed dissimilarity between replicates is affected by the choice of dissimilarity index**  
 323 Both the AGS and MFC samples contained microbial community replicates, which means that DNA  
 324 was extracted in parallel from six aliquots of biomass collected from the same microbial community  
 325 (e.g. the same AGS reactor or the same MFC biofilm). The MFC samples also contained one set of  
 326 technical replicates, which in this study means that the same DNA extract was processed in six  
 327 separate PCR reactions followed by sequencing of the six separate PCR products.

328  
 329 The diversity order ( $q$ ) of the dissimilarity index had a strong effect on the dissimilarity between  
 330 replicates. The highest dissimilarity was observed for incidence-based indices ( $^0d$  and Jaccard) and the  
 331 dissimilarity typically decreased with increasing diversity order (**Fig. 3**). Overall, the technical  
 332 replicates had lower dissimilarity than the community replicates for diversity order from 0 to 2 ( $p <$   
 333  $0.05$ ,  $n=15$ , Welch's anova). The consensus table had lower dissimilarity between replicates than the  
 334 two count tables used to generate the consensus table at low diversity orders ( $q < 1$ ) for all seven sets  
 335 of community replicates as well as for the technical replicates (see **Fig. S2.12 in Additional file 2**).  
 336

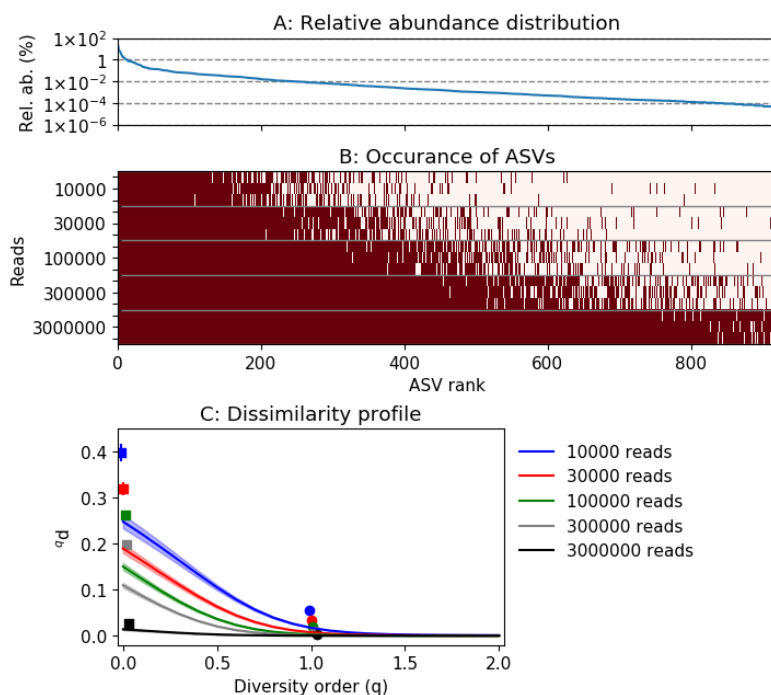


337  
 338 **Fig. 3.** Dissimilarities between replicates ( $n=6$ ). (A) A comparison between the community- and technical  
 339 replicates for samples from the MFC experiment. (B) Other community replicates from the MFC experiment  
 340 and (C) community replicates from the AGS experiment. Hill-based dissimilarity values ( ${}^q d$ ) are shown as lines.  
 341 Jaccard and Bray-Curtis dissimilarities are shown as squares and circles, respectively. Shaded regions and error  
 342 bars are standard deviations of pairwise dissimilarities ( $n=15$ ). The MFC data set had four categories of  
 343 samples: acetate-fed biofilms growing on anodes (Ac.anod.), acetate-fed biofilms growing on non-conductive  
 344 surfaces (Ac.non-cond.), glucose-fed biofilms growing on anodes (Glu.anod.), and glucose-fed biofilms growing  
 345 on non-conductive surfaces (Glu.non-cond.). The AGS data set had three sample categories: the inoculum  
 346 (Inoc), reactor 1 (R1), and reactor 2 (R2). The technical replicates were taken from a Glu.anod. sample.

347  
 348 **Random sampling affects the observed dissimilarity between replicates**

349 The high dissimilarity between replicates for low diversity orders could be the result of  
 350 undersampling [47]. To examine this effect, we used a simulation. The AGS data set served as a  
 351 hypothetical case. **Fig. 4A** shows the relative abundance distribution of the 919 ASVs found in the  
 352 AGS consensus table. Let us assume this represents the true relative abundances of all taxa present in  
 353 the investigated microbial community. Five sets of samples with sequencing depths ranging from  
 354 10 000 to 3 million reads per samples were obtained from the community. The samples were  
 355 generated by random sampling with replacement from the relative abundance distribution. Increasing  
 356 sequencing depth led to increasing number of detected ASVs (**Fig. 4B**). The average pairwise  
 357 dissimilarity between six replicate samples is shown in **Fig. 4C**. The curves have the same shape as  
 358 the experimentally observed dissimilarities in **Fig. 3**. A sequencing depth of 300 000, which is similar  
 359 to the actual sequencing depth for the AGS data set (278 758 reads/sample), generated approximately  
 360 the same dissimilarity profile as the real data (see **Fig. 3C and 4C**). The detection of the ASVs

361 increased and the dissimilarity between replicates decreased with increasing sequencing depth (**Fig.**  
 362 **S2.13, Additional file 2**). At a sequencing depth of 3 million reads, 98.5±0.4% of the ASVs were  
 363 detected.  
 364



365 **Fig. 4.** Simulation of the effect of sequencing depth on dissimilarity between replicates. (A) Relative abundance  
 366 distribution for the microbial community being sampled. (B) ASVs detected in samples having different  
 367 sequencing depths. Dark red color indicates that the ASV was detected. Three samples are shown for each  
 368 sequencing depth. (C) Average pairwise dissimilarities between replicate samples at each sequencing depth. The  
 369 shaded regions show the standard deviations (n=15). Jaccard- and Bray-Curtis dissimilarities are shown as  
 370 squares and circles, respectively.  
 371

372  
 373 **Effect of the choice of diversity index on observed differences between sample categories**  
 374 The ability of different dissimilarity indices to distinguish between sample categories in the  
 375 experimental data was also tested. The AGS data set was more challenging than the MFC data set  
 376 because most taxa were shared between different samples. Therefore, the AGS consensus table with  
 377 the three sample categories, the inoculum, reactor 1 (R1), and reactor 2 (R2), was used in the analysis.  
 378 The F-statistic is the ratio of between-group variability and within-group variability. Dissimilarity  
 379 matrices resulting in the calculation of a high F-statistic are thus better at resolving differences  
 380 between sample categories. Dissimilarity matrices generated with the <sup>1</sup>d and <sup>2</sup>d indices resulted in F-  
 381 statistics of 2492 and 2969, respectively. The Bray-Curtis index resulted in an F-statistic of 153. The  
 382 incidence-based <sup>0</sup>d and Jaccard indices resulted in values of 20 and 15, respectively. High  
 383 dissimilarity between replicates, which was observed for the incidence-based indices (**Fig. 3**), would  
 384 result in lower F-statistic. Despite large differences in the F-statistic, statistically significant  
 385 separation between the three sample categories was found with all dissimilarity indices (permanova,  
 386 p=0.001, 999 permutations) (see also **Text S2.4 in Additional file 2**). A PCoA showing separation  
 387 between the sample categories using the <sup>0</sup>d index is shown in **Fig. S2.11 (Additional file 2)**.  
 388

389 **The choice of dissimilarity index influence hypothesis testing**

390  
 391 *AGS experiment*

392 In the AGS experiment, we hypothesized that R1 and R2 diverged from the inoculum to the same  
 393 extent after 150 days of operation since they were operated under identical condition and had similar

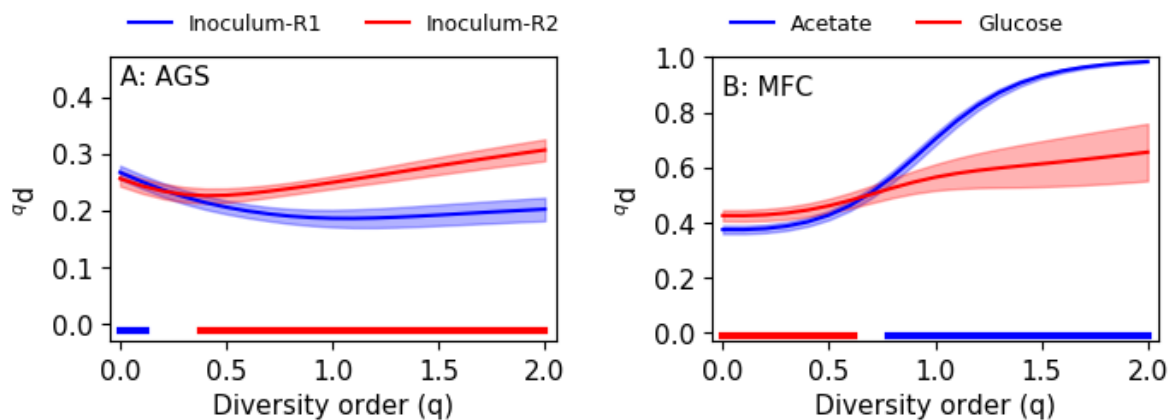
394 performance. Thus, the dissimilarity between the inoculum and R1 should be the same as between the  
 395 inoculum and R2. The results are shown in **Fig. 5A**. For high diversity orders ( $q \geq 0.4$ ), the  
 396 dissimilarity between the inoculum and R2 is larger than between the inoculum and R1 and for low  
 397 diversity order ( $q \leq 0.1$ ), higher dissimilarity is observed between the inoculum and R1 ( $p < 0.05$ ,  
 398 Welch's anova). However, it should be noted that the magnitude of the difference is small at low  
 399 diversity order.

400

401 *MFC experiment*

402 In the MFC experiment, we compared microbial communities of electroactive biofilms growing on  
 403 anodes with biofilms growing on non-conductive porous separators. We hypothesized that biofilms  
 404 growing on conductive and non-conductive surfaces would be more dissimilar to each other in the  
 405 acetate-fed MFC than in the glucose-fed MFC. Glucose is a fermentable substrate and fermentative  
 406 microorganisms should be able to grow anywhere within the MFCs, leading to a more homogenous  
 407 microbial community structure. Acetate, on the other hand, is non-fermentable and the microbial  
 408 communities in an acetate-fed MFC are therefore dependent on electron acceptor availability. On the  
 409 anode surface, the anode serves as electron acceptor while in other locations within the MFCs, the  
 410 microorganisms must use soluble compounds such as oxygen diffusing in through the gas-diffusion  
 411 cathode. Microbial communities in different locations of the acetate-fed MFCs should therefore have  
 412 different metabolisms, which likely leads to higher dissimilarity than between communities within the  
 413 glucose-fed MFCs which, at least partly, could have the same metabolism, namely fermentation [32].  
 414 For high diversity orders, ( $q \geq 0.8$ ), there was higher dissimilarity in the acetate-fed MFC than in the  
 415 glucose-fed MFC. For low diversity orders ( $q \leq 0.6$ ), the glucose-fed MFC had higher dissimilarity ( $p$   
 416  $< 0.05$ , Welch's anova) (**Fig. 5B**).

417



418

419 **Fig. 5.** (A) Average pairwise dissimilarity between the inoculum and R1, and the inoculum and R2 for the AGS  
 420 data set. (B) Average pairwise dissimilarity between the electroactive biofilm growing in the anode and the  
 421 biofilm growing on the non-conductive separator in the acetate-fed and glucose-fed MFCs. Shaded regions show  
 422 standard deviations. The horizontal bars near the x-axis indicate significant difference in dissimilarity (Welch's  
 423 anova,  $p < 0.05$ ,  $n=36$ ). The color of the bar shows which pair has the highest dissimilarity.

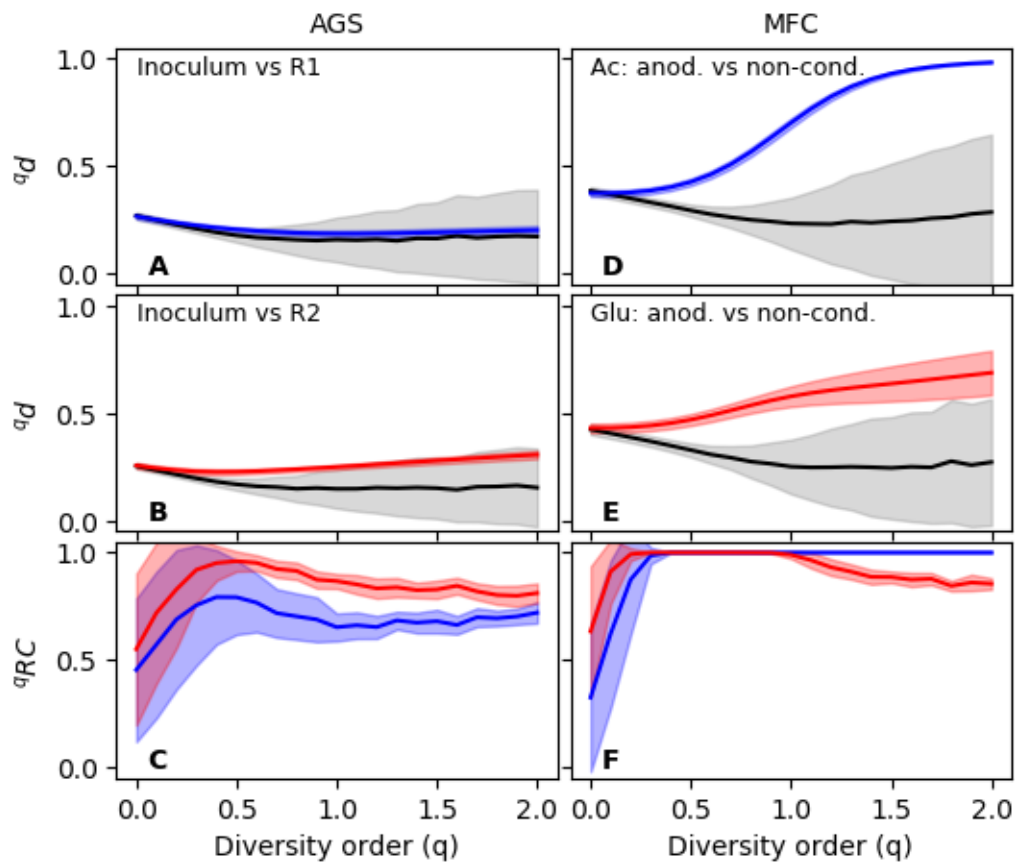
424

425 *Null model*

426 Null models were used to aid in the interpretation of dissimilarity values. The results from the AGS  
 427 experiment is shown in **Fig. 6A-C**. The dissimilarity between the inoculum and R1 is not significantly  
 428 different from the null distribution at any diversity order and consequently  ${}^9RC$  is close to 0.5. For the  
 429 inoculum and R2, the observed dissimilarity is higher than between the inoculum and R1; however,  
 430 the null expectation of random assembly could not be rejected at a significance level of 0.05.

431

432 For the MFC data set, the results from the null model analysis are shown in **Fig. 6D-F**. At a diversity  
 433 order of 0, the observed dissimilarity is similar to the null expectation and consequently  ${}^q\text{RC}$  is close  
 434 to 0.5. This indicates that if we only care about presence/absence of ASVs, there is a random  
 435 distribution between the two biofilm communities. With increasing emphasis on relative abundance,  
 436 the dissimilarity between biofilm types is higher than the null distribution. For the acetate-fed MFCs,  
 437 the  ${}^q\text{RC}$  values are close to 1, which means significant compositional differences between the two  
 438 communities. For the glucose-fed MFCs, the  ${}^q\text{RC}$  again drops to lower values at a diversity order  
 439 above 1. This means that some of the most abundant ASVs are shared between biofilms growing on  
 440 conductive and non-conductive surfaces. This indeed turned out to be the case with a *Trichococcus* sp.  
 441 being highly abundant in both biofilm communities, likely carrying out fermentation in both places  
 442 [32].  
 443



444 **Figure 6.** Null model simulation (199 randomizations). (A-C) Results for the AGS data set. (D-F) Results for  
 445 the MFC data set. (A) Dissimilarity between the inoculum and R1 (blue) in comparison to the null distribution  
 446 (black). (B) Dissimilarity between the inoculum and R2 (red) in comparison to the null distribution (black). (C)  
 447  ${}^q\text{RC}$  values for the inoculum-R1 (blue) and inoculum-R2 (red) comparisons. (D) Dissimilarity between biofilms  
 448 on anodes and non-conductive surfaces in the acetate-fed MFC (blue) in comparison to the null distribution  
 449 (black). (E) Dissimilarity between biofilms on anodes and non-conductive surfaces in the glucose-fed MFC  
 450 (red) in comparison to the null distribution (black). (F)  ${}^q\text{RC}$  values for the biofilm comparisons in the acetate-fed  
 451 MFC (blue) and glucose-fed MFC (red). Shaded regions show standard deviations based on all pairwise  
 452 comparisons ( $n=36$ ).  
 453

454

## 455 DISCUSSION

456

### 457 **A consensus count table removes many low-abundant ASVs but retains most of the reads**

458 Previous studies comparing bioinformatics pipelines for high-throughput sequencing of marker-genes  
459 have found large differences in alpha diversity estimates [42, 48-51]. We also observed that both the  
460 pipeline and the input parameter values chosen by the user affected the number of inferred  
461 OTUs/ASVs as well as the number of reads mapped to these (see **Fig. S2.1-2 in Additional file 2**).  
462 With real samples of unknown composition, it is difficult to choose which pipeline and which settings  
463 to use for the analysis. A way to approach the problem of inflated OTU/ASV counts is to infer a  
464 consensus table based on OTUs/ASVs detected using several different pipelines. We have  
465 implemented an algorithm for doing this in qdiv. Running the algorithm with DADA2 and UNOISE  
466 count tables as input resulted in dramatic drops in the ASV count in the consensus tables; however,  
467 most of the reads (99.4-99.7%) were associated with the consensus ASVs.

468

### 469 **Dissimilarity between replicates depends on the diversity order and can be explained by** 470 **random sampling effects**

471 High dissimilarity between replicates can make it difficult to use marker-gene amplicon sequencing to  
472 distinguish categories of samples. For example, Bautista-de los Santos et al. [52] studied microbial  
473 communities in drinking water using the Jaccard and Bray-Curtis indices on an OTU table generated  
474 with Mothur. Fewer significant differences between sample categories were observed with the Jaccard  
475 index because of high dissimilarity between replicate samples [52]. We also observed much lower F  
476 statistics for the AGS data set with incidence-based dissimilarity indices, which was caused by higher  
477 dissimilarity between community replicates in relation to dissimilarity between sample categories.

478

479 Dissimilarity between replicates can be caused by many factors associated with sampling, DNA  
480 extraction, PCR, sequencing, and data processing [53]. The comparison between community- and  
481 technical replicates in **Fig. 3A** suggested that only a relatively small fraction was associated with  
482 sampling and DNA extraction for the case of an MFC biofilm sampled from an anode. The  
483 dissimilarity of replicates was the highest for incidence-based indices and low diversity order ( $q < 1$ ),  
484 which means that low-abundant OTUs/ASVs had a strong influence on the observed dissimilarity.  
485 The species-abundance distribution of microbial communities can contain a long tail of low-abundant  
486 taxa of which only some may be detected in the analyzed samples. This random sampling effect [5,  
487 47], as well as the generation of erroneous OTUs/ASVs during PCR, sequencing and data processing,  
488 cause dissimilarity between replicates. The random sampling effect was shown using a simulation in  
489 **Fig. 4**, where the simulated dissimilarity between replicates corresponded very well with the  
490 experimentally observed dissimilarity at a sequencing depth of approximately 300 000 reads/sample.

491

492 Previously, Haegeman et al. [31] showed the difficulty of estimating alpha diversity at low diversity  
493 orders ( $q < 1$ ) because even in deeply sequenced samples, we lack information about the tail of low-  
494 abundant OTUs/ASVs. In the simulation in **Fig. 4**, the true dissimilarity was 0 since all samples were  
495 collected from the same hypothetical community. However, the simulated dissimilarity for low  
496 diversity orders ( $q < 1$ ) was much higher than 0, although it decreased as sample size increased.

497

498 **Fig. 3-5** show dissimilarity as a function of diversity order. The mean and standard deviation of  
499 several pairwise comparisons of samples from the compared communities are shown in each figure.  
500 Although we know that the calculated dissimilarities at low diversity order are likely incorrect, the  
501 standard deviations (shaded regions) are generally very small. This means that for a given sample size  
502 (sequencing depth), the calculated dissimilarity is reproducible. It does not mean that the calculated  
503 dissimilarity is a good estimate of the true dissimilarity between the microbial communities from  
504 which the samples were taken. For example, **Fig. 4** shows the mean and standard deviation of 15

505 pairwise dissimilarity values between six simulated samples. The standard deviation of the simulated  
506 dissimilarity is very small, but the mean is far from the true value. For a sample size of 300 000 reads,  
507  $^0d$  was  $0.11 \pm 0.01$ . However, in this case we know that the true dissimilarity was 0.

508  
509 The dissimilarity between replicates decreased with increasing diversity order until  $q$  was  
510 approximately one (**Fig. 3**). For some samples, most notably the biofilm samples from non-conductive  
511 surfaces in the MFC experiment, the dissimilarity between replicates then increased at higher  
512 diversity order and for the Bray-Curtis index (**Fig. 3B**). At low diversity order ( $q < 1$ ), the dissimilarity  
513 between replicates could be lowered by generating a consensus table (**Fig. S2.12, Additional file 2**).  
514 The consensus table excludes many low-abundant and potentially spurious ASVs were from the data  
515 sets. Since low-abundant OTUs/ASVs have a large impact on low diversity order dissimilarity  
516 indices, dropping some of them from the data set leads to reduced dissimilarity. At a high diversity  
517 order (e.g.  $q=2$ ), the calculated dissimilarity is highly dependent on the relative abundance of the most  
518 abundant OTUs/ASVs in each sample. Small differences in relative abundance values of those  
519 OTUs/ASVs are amplified, which leads to increasing dissimilarity. In the MFC sample, heterogeneity  
520 of the biofilms growing on the non-conductive surfaces may have caused the observed dissimilarity  
521 between community replicates at high diversity order. The  $^1d$  index, which weighs OTUs/ASVs  
522 exactly according to their relative abundance in the sample, seems to be a good compromise leading  
523 to low dissimilarity between replicates and hence better possibilities of detecting actual differences  
524 between samples collected from microbial communities exposed to different treatments.

#### 525 526 **Hypotheses should be tested for a range of diversity orders to determine the effects of taxa with** 527 **different relative abundances**

528 Previous research has shown that Hill numbers are suitable for quantifying alpha diversity in samples  
529 obtained by high-throughput sequencing of marker-genes [29]. For example, Haegeman et al. [31]  
530 analyzed alpha diversity as a function of diversity order and concluded that Hill numbers with  $q > 1$   
531 give robust estimates of alpha diversity. In this study, we show that dissimilarity profiles, which show  
532 the dissimilarity between samples as a function of diversity order (**Fig. 5**), are highly informative also  
533 in the study of beta diversity. The use of a single dissimilarity index would have given misleading  
534 information for the data sets investigated in this study. In the AGS experiment, incidence-based  
535 indices showed that R1 and R2 were about equally dissimilar to the inoculum. However, at higher  
536 diversity order, there was a clear difference. In the MFC experiment, the incidence-based indices  
537 would have led us to conclude that the dissimilarity between biofilms on conductive and non-  
538 conductive surfaces in the acetate-fed MFCs was lower than in the glucose-fed MFCs, contrary to our  
539 hypothesis. However, when we plot dissimilarity as a function of  $q$ , we see that when we focus on the  
540 more abundant OTUs/ASVs ( $q > 1$ ), the bioanodes and biofilms in the glucose-fed MFCs are in fact  
541 less dissimilar, in line with our hypothesis.

542  
543 Contrary to the commonly used Bray-Curtis index, the Hill-based dissimilarity indices have an  
544 intuitive interpretation. The  $^q d$  index quantifies the effective average proportion of OTUs/ASVs in one  
545 sample *not shared* with the other sample [54]. If two samples have  $S$  number of equally common  
546 OTUs/ASVs and  $C$  of them are shared, the dissimilarity value would be  $1-C/S$  [25]. Thus, the number  
547 itself has a meaning. For example,  $^0 d$  can be interpreted as the average proportion of all OTUs/ASVs-,  
548  $^1 d$  as the average proportion of “common” OTUs/ASVs-, and  $^2 d$  as the average proportion of  
549 “abundant” OTUs/ASVs *not shared* between two samples.

550  
551 The Hill-based dissimilarity indices can also be extended to take relationships between OTUs/ASVs  
552 into account [54]. Using either a phylogenetic tree or a matrix of pairwise distances as input,  
553 phylogenetic- or functional dissimilarity indices can be calculated [26, 55, 56]. As phylogenetically  
554 closely related taxa tend to have similar functional capabilities and habitat preferences [57],  
555 dissimilarity indices that take phylogenetic relatedness into account could, in comparison to

556 taxonomic indices, provide more information about functional differences between microbial  
557 communities.

558

559 Null models help us to further interpret the meaning of the dissimilarity values. The data set from the  
560 MFCs show that for a diversity order of 0, the distribution of OTUs/ASVs between the two types of  
561 biofilms is close to the null expectation. This is logical considering that the two biofilms are  
562 physically located close to each other and linked by dispersal. There is, thus, a high likelihood that the  
563 same OTUs/ASVs can be detected in both locations, even if they do not grow in both locations. For  
564 higher diversity order (i.e.  $q=1$ ) we see a higher dissimilarity than the null expectation, suggesting that  
565 the common OTUs/ASVs are different in the two locations. This could be explained by heterogeneous  
566 selection. The conductive anode surface selects for electroactive microorganisms whereas the non-  
567 conductive separator selects for oxygen scavengers. For even higher diversity order ( $q = 2$ ), the  
568 dissimilarity between the two biofilms in the glucose-fed MFC again approaches the null expectation.  
569 This is logical considering that one of the most abundant taxa in the glucose-fed MFCs was a  
570 fermentative *Trichococcus* sp., which could grow in both locations [32].

571

## 572 CONCLUSIONS

- 573 • Bioinformatics pipelines ran with different settings resulted in count tables having large  
574 differences in the number of OTUs/ASVs and total reads. A way to minimize the effect of  
575 low-abundant and possibly spurious OTUs/ASVs on the analysis is to generate a consensus  
576 table based on several other count tables generated using different denoising pipelines (e.g.  
577 UNOISE, DADA2, and Deblur).
- 578 • Conclusions drawn from experimental data can depend on the chosen dissimilarity index. To  
579 fully understand beta diversity patterns, Hill-based dissimilarity values should be calculated  
580 for several diversity orders ( $q$ ). Dissimilarity profiles plotting  $^q d$  as a function of  $q$  are  
581 informative.
- 582 • Null models, which can be calculated based on all dissimilarity indices, help in the  
583 interpretation of dissimilarity values and give information about community assembly  
584 mechanisms.
- 585 • The Python package `qdiv`, freely available at <https://github.com/omvatten/qdiv> with  
586 documentation at <https://qdiv.readthedocs.io/en/latest/>, enables simple calculation of Hill-  
587 based dissimilarity indices and associated null models. It can also be used to calculate  
588 consensus count tables.

589

## 590 METHODS

591

### 592 Experimental

593 Samples collected from two separate experiments were analyzed in this study. In the AGS  
594 experiment, granular sludge from a sequencing batch reactor was used to inoculate two new reactors  
595 (R1 and R2). Six samples were collected from the inoculum as well as from each of the two new  
596 reactors after 150 days of operation (**Fig. S3.1, Additional file 3**). The sets of six are called  
597 community replicates. Reactor R1 and R2 had similar performance over time with total organic  
598 carbon removal  $>90\%$  and total nitrogen removal of  $35.2\pm 14.6\%$  in R1 and  $37.0\pm 12.7\%$  in R2. They  
599 also had similar average granule size in the end of the experiment and followed the same trajectory in  
600 terms of suspended solids concentrations in the reactors.

601

602 In the MFC experiment, parallel MFCs were operated with either acetate or glucose as the sole  
603 electron donor [for details, see 32]. Samples were collected from the anode where a biofilm of  
604 electroactive microorganisms oxidized the electron donor and generated electrical current, and from a  
605 non-conductive porous separator where a biofilm oxidized or fermented the electron donor and



606 scavenged oxygen (**Fig. S3.2 Additional file 3**). In one acetate- and one glucose-fed MFC, the  
607 biofilm samples were each cut into six pieces and DNA was extracted and processed separately from  
608 each piece. These samples are called community replicates. The DNA extracted from one of the  
609 anode-attached biofilm samples was also processed in six separate PCR reactions. These samples are  
610 called technical replicates.

611

612 DNA was extracted using the FastDNA Spin Kit for Soil (MP Biomedicals). PCR amplification of the  
613 V4 region of the 16S rRNA gene was carried out with the primer pair 515'F  
614 (GTGBCAGCMGCCGCGGTAA) and 806R (GGACTACHVGGGTWTCTAAT) [58, 59] and the  
615 dual indexing strategy by Kozich et al. [3]. High-throughput sequencing was carried out using the  
616 Illumina MiSeq platform and reagent kit V3 (2x300 bp paired-end sequencing). Further details are  
617 provided in **Text S3.1 (Additional file 3)**. The samples from the AGS and MFC experiments were  
618 processed in two separate sequencing runs. The sequencing results were deposited in the European  
619 Nucleotide Archive with accession numbers PRJEB35721 (AGS data set) and PRJEB26776 (MFC  
620 data set). The specific run accession numbers for each pair of fastq files used in the study and the  
621 corresponding sample identities are shown in **Tables S3.1-2 (Additional file 3)**.

622

### 623 **Bioinformatics**

624 The sequence reads were processed using DADA2 version 1.10 [43], Deblur version 1.04 [44],  
625 USEARCH version 10 [45], and Mothur version 1.41 [46]. The pipelines offer the user various  
626 choices. For example, the stringency of the quality filtering method can typically be varied, and the  
627 reads can often be processed either separately sample-by-sample or in pooled mode. Analysis of  
628 pooled samples requires more computer memory. DADA2 and Deblur generate ASVs whereas  
629 Mothur generate OTUs. USEARCH can either generate ASVs using UNOISE [60] or OTUs using  
630 UPARSE [61]. Several count tables were generated using various input parameter settings in the  
631 pipelines (**see Additional file 2**). Details about the pipelines are provided at  
632 [github.com/omvatten/amplicon\\_sequencing\\_pipelines](https://github.com/omvatten/amplicon_sequencing_pipelines). DADA2 and UNOISE count tables were used  
633 to generate consensus tables consisting of ASVs detected using both pipelines. This was done with a  
634 function implemented in qdiv.

635

### 636 **Software**

637 A software, qdiv, allowing calculation of all the indices and null models mentioned above was  
638 developed in Python3 and is available as a Python package. It makes use of the following Python  
639 packages: pandas [62], numpy [63], matplotlib [64], and python-Levenshtein. The source code for  
640 qdiv is available at <https://github.com/omvatten/qdiv>. It is available via PyPI and the Anaconda cloud.

641

### 642 **Statistical analysis**

643 To determine statistical significance of the association between different dissimilarity matrices,  
644 Mantel's permutation test was used [65]. To compare the variability within sample categories to the  
645 variability between samples categories, permanova was used [66]. Both the Mantel test and  
646 permanova were implemented in qdiv. Welch's anova was carried out using SciPy [67].

647

### 648 **Null model**

649 In the AGS experiment, we defined all samples from the inoculum, R1, and R2 as the regional pool.  
650 In the MFC experiment, we were interested in the dissimilarity between the anode biofilm and biofilm  
651 growing on a non-conductive surface within the same MFC. Thus, we defined all samples collected  
652 from one specific MFCs as one regional pool. For randomization scheme, we used the frequency  
653 approach, which is the same as in Stegen et al. [41]. Briefly, the number of OTUs/ASVs and reads in  
654 a sample are recorded. The null version of the sample is generated by randomly picking the same  
655 number of OTUs/ASVs from the regional pool. The likelihood of being picked corresponds to the  
656 frequency of samples in which the OTU/ASV is found. The picked OTUs/ASVs are then populated

657 with reads so that the total number of reads in the randomly assembled sample equals that of the real  
658 sample. The likelihood for a read of being picked is related to the total number of reads associated  
659 with the OTUs/ASVs in the regional pool.

660

661 It should be noted that the  ${}^q\text{RC}$  value defined in Eq. 4 is constrained between 0 and 1. If a range  
662 between -1 and 1 is desired, e.g. as in Chase et al. [36], this can be accomplished by subtracting 0.5  
663 from the  ${}^q\text{RC}$  value, and multiplying by 2.

664

665 **DECLARATIONS**

666

667 **Ethics approval and consent to participate**

668 Not applicable

669

670 **Consent to publication**

671 Not applicable

672

673 **Availability of data and materials**

674 Amplicon sequence data are deposited at the European Nucleotide Archive under accession numbers  
675 PRJEB35721 (AGS data set) and PRJEB26776 (MFC data set). Sample identities corresponding to  
676 the run accession numbers are provided in Table S3.1-2 (Additional file 3).

677 Bioinformatics pipelines used to process the sequence data and generate count tables are available at  
678 [https://github.com/omvatten/amplicon\\_sequencing\\_pipelines](https://github.com/omvatten/amplicon_sequencing_pipelines). Information about the execution of the  
679 pipelines is also provided in Text S2.1 (Additional file 2).

680 The code for qdiv, which was the software developed in this project and used to analyze the count  
681 tables is available at <https://github.com/omvatten/qdiv>.

682

683 **Competing interests**

684 The authors declare that they have no competing interests.

685

686 **Funding**

687 The project was funded by the Swedish Research Council (VR, grant 2012-5167) and the Swedish  
688 Research Council for Environment, Agricultural Sciences, and Spatial Planning (FORMAS, grant  
689 2013-627, grant 2018-01423, and grant 2018-0622).

690

691 **Authors' contributions**

692 OM and SS operated the MFCs and generated the sequence data for that experiment. RL operated the  
693 AGS reactors and generated the sequence data for the experiment. OM developed the software and  
694 was the main author of the manuscript. All authors critically reviewed and approved the final  
695 manuscript.

696

697 **Acknowledgements**

698 The authors acknowledge the Genomics core facility at the University of Gothenburg for support and  
699 use of their equipment. Two anonymous reviewers provided important comments allowing us to  
700 improve the article.

701

702

703

704 **References**

- 705 1. Locey KJ, Lennon JT: **Scaling laws predict global microbial diversity**. *PNAS* 2016,  
706 **113**(21):5970-5975.
- 707 2. Caporaso JG, Lauber CL, Walters WA, Berg-Lyons D, Huntley J, Fierer N, Owens SM, Betley J,  
708 Fraser L, Bauer M *et al*: **Ultra-high-throughput microbial community analysis on the**  
709 **Illumina HiSeq and MiSeq platforms**. *ISME Journal* 2012, **6**(8):1621-1624.
- 710 3. Kozich JJ, Westcott SL, Baxter NT, Highlander SK, Schloss PD: **Development of a dual-index**  
711 **sequencing strategy and curation pipeline for analyzing amplicon sequence data on the**  
712 **MiSeq Illumina sequencing platform**. *Applied and Environmental Microbiology* 2013,  
713 **79**(17):5112-5120.
- 714 4. Aigle A, Prosser JI, Gubry-Rangin C: **The application of high-throughput sequencing**  
715 **technology to analysis of amoA phylogeny and environmental niche specialisation of**  
716 **terrestrial bacterial ammonia-oxidisers**. *Environmental Microbiome* 2019, **14**(1):3.
- 717 5. Zhou J, Jiang Y-H, Deng Y, Shi Z, Zhou BY, Xue K, Wu L, He Z, Yang Y: **Random sampling**  
718 **process leads to overestimation of  $\beta$ -diversity of microbial communities**. *mBio* 2013,  
719 **4**(3):e00324-00313.
- 720 6. Fouhy F, Clooney AG, Stanton C, Claesson MJ, Cotter PD: **16S rRNA gene sequencing of**  
721 **mock microbial populations- impact of DNA extraction method, primer choice and**  
722 **sequencing platform**. *BMC microbiology* 2016, **16**(1):123-123.
- 723 7. Kembel SW, Wu M, Eisen JA, Green JL: **Incorporating 16S gene copy number information**  
724 **improves estimates of microbial diversity and abundance**. *PLOS Computational Biology*  
725 2012, **8**(10):e1002743.
- 726 8. Gonzalez JM, Portillo MC, Belda-Ferre P, Mira A: **Amplification by PCR artificially reduces**  
727 **the proportion of the rare biosphere in microbial Communities**. *PLOS One* 2012,  
728 **7**(1):e29973.
- 729 9. Schloss PD, Gevers D, Westcott SL: **Reducing the effects of PCR amplification and**  
730 **sequencing artifacts on 16S rRNA-based studies**. *PLoS One* 2011, **6**(12):e27310.
- 731 10. Eren AM, Morrison HG, Lescault PJ, Reveillaud J, Vineis JH, Sogin ML: **Minimum entropy**  
732 **decomposition: unsupervised oligotyping for sensitive partitioning of high-throughput**  
733 **marker gene sequences**. *ISME Journal* 2015, **9**(4):968-979.
- 734 11. Rosen MJ, Callahan BJ, Fisher DS, Holmes SP: **Denoising PCR-amplified metagenome data**.  
735 *BMC Bioinformatics* 2012, **13**(283).
- 736 12. Tikhonov M, Leach RW, Wingreen NS: **Interpreting 16S metagenomic data without**  
737 **clustering to achieve sub-OTU resolution**. *ISME Journal* 2015, **9**(1):68-80.
- 738 13. García-García N, Tamames J, Linz AM, Pedrós-Alió C, Puente-Sánchez F: **Microdiversity**  
739 **ensures the maintenance of functional microbial communities under changing**  
740 **environmental conditions**. *ISME journal* 2019.
- 741 14. He Y, Caporaso JG, Jiang X-T, Sheng H-F, Huse SM, Rideout JR, Edgar RC, Kopylova E, Walters  
742 WA, Knight R *et al*: **Stability of operational taxonomic units: an important but neglected**  
743 **property for analyzing microbial diversity**. *Microbiome* 2015, **3**(1):20.
- 744 15. Callahan BJ, McMurdie PJ, Holmes SP: **Exact sequence variants should replace operational**  
745 **taxonomic units in marker-gene data analysis**. *ISME Journal* 2017.
- 746 16. Koleff P, Gaston KJ, Lennon JJ: **Measuring beta diversity for presence-absence data**. *Journal*  
747 *of Animal Ecology* 2003, **72**(3):367-382.
- 748 17. Barwell LJ, Isaac NJB, Kunin WE: **Measuring  $\beta$ -diversity with species abundance data**.  
749 *Journal of Animal Ecology* 2015, **84**(4):1112-1122.
- 750 18. Porter TM, Hajibabaei M: **Scaling up: A guide to high-throughput genomic approaches for**  
751 **biodiversity analysis**. *Molecular Ecology* 2018, **27**(2):313-338.
- 752 19. Escolà Casas M, Nielsen TK, Kot W, Hansen LH, Johansen A, Bester K: **Degradation of**  
753 **mecoprop in polluted landfill leachate and waste water in a moving bed biofilm reactor**.  
754 *Water Research* 2017, **121**:213-220.

- 755 20. Kunin V, Engelbrektsen A, Ochman H, Hugenholtz P: **Wrinkles in the rare biosphere: pyrosequencing errors can lead to artificial inflation of diversity estimates.** *Environmental Microbiology* 2010, **12**(1):118-123.
- 756
- 757
- 758 21. McKnight DT, Huerlimann R, Bower DS, Schwarzkopf L, Alford RA, Zenger KR: **Methods for normalizing microbiome data: An ecological perspective.** *Methods in Ecology and Evolution* 2019, **10**(3):389-400.
- 759
- 760
- 761 22. Alberdi A, Gilbert MTP: **A guide to the application of Hill numbers to DNA-based diversity analyses.** *Molecular Ecology Resources* 2019, **19**(4):804-817.
- 762
- 763 23. Hill MO: **Diversity and evenness: A unifying notation and its consequences.** *Ecology* 1973, **54**(2):427-432.
- 764
- 765 24. Jost L: **Entropy and diversity.** *Oikos* 2006, **113**(2):363-375.
- 766 25. Jost L: **Partitioning diversity into independent alpha and beta components.** *Ecology* 2007, **88**(10):2427-2439.
- 767
- 768 26. Chiu CH, Jost L, Chao A: **Phylogenetic beta diversity, similarity, and differentiation measures based on Hill numbers.** *Ecological Monographs* 2014, **84**(1):21-44.
- 769
- 770 27. Chao A, Chiu C-H: **Bridging the variance and diversity decomposition approaches to beta diversity via similarity and differentiation measures.** *Methods in Ecology and Evolution* 2016, **7**(8):919-928.
- 771
- 772
- 773 28. Ellison AM: **Partitioning diversity.** *Ecology* 2010, **91**(7):1962-1963.
- 774 29. Kang S, Rodrigues JL, Ng JP, Gentry TJ: **Hill number as a bacterial diversity measure framework with high-throughput sequence data.** *Scientific Reports* 2016, **6**:38263.
- 775
- 776 30. Ma Z: **Measuring microbiome diversity and similarity with Hill numbers.** In: *Metagenomics*. Edited by Nagarajan M: Academic Press; 2018: 157-178.
- 777
- 778 31. Haegeman B, Hamelin J, Moriarty J, Neal P, Dushoff J, Weitz JS: **Robust estimation of microbial diversity in theory and in practice.** *ISME journal* 2013, **7**(6):1092-1101.
- 779
- 780 32. Saheb-Alam S, Persson B, Wilén B-M, Hermansson M, Modin O: **Response to starvation and microbial community analysis in microbial fuel cells enriched on different electron donors.** *Microbial Biotechnology* 2019, **12**(5):962-975.
- 781
- 782
- 783 33. Liébana R, Modin O, Persson F, Szabó E, Hermansson M, Wilén B-M: **Combined deterministic and stochastic processes control microbial succession in replicate granular biofilm reactors.** *Environmental Science & Technology* 2019, **53**(9):4912-4921.
- 784
- 785
- 786 34. Horner-Devine MC, Lage M, Hughes JB, Bohannan BJM: **A taxa-area relationship for bacteria.** *Nature* 2004, **432**(7018):750-753.
- 787
- 788 35. Baselga A: **Partitioning the turnover and nestedness components of beta diversity.** *Global Ecology and Biogeography* 2010, **19**(1):134-143.
- 789
- 790 36. Chase JM, Kraft NJB, Smith KG, Vellend M, Inouye BD: **Using null models to disentangle variation in community dissimilarity from variation in  $\alpha$ -diversity.** *Ecosphere* 2011, **2**(2):24.
- 791
- 792 37. Chase JM, Myers JA: **Disentangling the importance of ecological niches from stochastic processes across scales.** *Philosophical Transactions of the Royal Society B* 2011, **366**(2351-2363).
- 793
- 794
- 795 38. Raup DM, Crick RE: **Measurement of faunal similarity in paleontology.** *Journal of Paleontology* 1979, **53**(5):1213-1227.
- 796
- 797 39. Gotelli NJ, Graves GR: **Null models in ecology.** Washington and London: Smithsonian Institution Press; 1996.
- 798
- 799 40. Gotelli NJ, Ulrich W: **Statistical challenges in null model analysis.** *Oikos* 2012, **121**(2):171-180.
- 800
- 801 41. Stegen JC, Lin X, Fredrickson JK, Chen X, Kennedy DW, Murray CJ, Rockhold ML, Konopka A: **Quantifying community assembly processes and identifying features that impose them.** *ISME journal* 2013, **7**(11):2069-2079.
- 802
- 803

- 804 42. Nearing JT, Douglas GM, Comeau AM, Langille MGI: **Denoising the Denoisers: an**  
805 **independent evaluation of microbiome sequence error-correction approaches.** *PeerJ* 2018,  
806 **6:e5364.**
- 807 43. Callahan BJ, McMurdie PJ, Rosen MJ, Han AW, Johnson AJ, Holmes SP: **DADA2: High-**  
808 **resolution sample inference from Illumina amplicon data.** *Nature Methods* 2016, **13(7):581-**  
809 **583.**
- 810 44. Amir A, McDonald D, Navas-Molina JA, Kopylova E, Morton JT, Zech Xu Z, Kightley EP,  
811 Thompson LR, Hyde ER, Gonzalez A *et al*: **Deblur rapidly resolves single-nucleotide**  
812 **community sequence patterns.** *mSystems* 2017, **2(2).**
- 813 45. Edgar RC: **Search and clustering orders of magnitude faster than BLAST.** *Bioinformatics*  
814 2010, **26(19):2460-2461.**
- 815 46. Schloss PD, Westcott SL, Ryabin T, Hall JR, Hartmann M, Hollister EB, Lesniewski RA, Oakley  
816 BB, Parks DH, Robinson CJ *et al*: **Introducing mothur: Open-source, platform-independent,**  
817 **community-supported software for describing and comparing microbial communities.**  
818 *Applied and Environmental Microbiology* 2009, **75(23):7537-7541.**
- 819 47. Beck J, Holloway JD, Schwanghart W: **Undersampling and the measurement of beta**  
820 **diversity.** *Methods in Ecology and Evolution* 2013, **4(4):370-382.**
- 821 48. Allali I, Arnold JW, Roach J, Cadenas MB, Butz N, Hassan HM, Koci M, Ballou A, Mendoza M,  
822 Ali R *et al*: **A comparison of sequencing platforms and bioinformatics pipelines for**  
823 **compositional analysis of the gut microbiome.** *BMC Microbiology* 2017, **17(1):194.**
- 824 49. Plummer E, Twin J: **A comparison of three bioinformatics pipelines for the analysis of**  
825 **preterm gut microbiota using 16S rRNA gene sequencing data.** *Journal of Proteomics &*  
826 *Bioinformatics* 2015, **8(12).**
- 827 50. Pylro VS, Roesch LFW, Morais DK, Clark IM, Hirsch PR, Tótoia MR: **Data analysis for 16S**  
828 **microbial profiling from different benchtop sequencing platforms.** *Journal of*  
829 *Microbiological Methods* 2014, **107:30-37.**
- 830 51. Sinclair L, Osman OA, Bertilsson S, Eiler A: **Microbial community composition and diversity**  
831 **via 16S rRNA gene amplicons: evaluating the Illumina platform.** *PLOS One* 2015,  
832 **10(2):e0116955.**
- 833 52. Bautista-de los Santos QM, Schroeder JL, Blakemore O, Moses J, Haffey M, Sloan W, Pinto  
834 AJ: **The impact of sampling, PCR, and sequencing replication on discerning changes in**  
835 **drinking water bacterial community over diurnal time-scales.** *Water Research* 2016,  
836 **90:216-224.**
- 837 53. Zinger L, Bonin A, Alsos IG, Bálint M, Bik H, Boyer F, Chariton AA, Creer S, Coissac E, Deagle  
838 BE *et al*: **DNA metabarcoding—Need for robust experimental designs to draw sound**  
839 **ecological conclusions.** *Molecular Ecology* 2019.
- 840 54. Chao A, Chiu C-H, Jost L: **Unifying species diversity, phylogenetic diversity, functional**  
841 **diversity, and related similarity and differentiation measures through Hill numbers.** *Annu*  
842 *Rev Ecol Syst* 2014, **45:297-324.**
- 843 55. Chao A, Chiu C-H, Jost L: **Phylogenetic diversity measures based on Hill numbers.**  
844 *Philosophical Transactions of the Royal Society B: Biological Sciences* 2010, **365(1558):3599-**  
845 **3609.**
- 846 56. Chiu CH, Chao A: **Distance-based functional diversity measures and their decomposition: a**  
847 **framework based on Hill numbers.** *PLoS One* 2014, **9(7):e100014.**
- 848 57. Morrissey EM, Mau RL, Schwartz E, Caporaso JG, Dijkstra P, van Gestel N, Koch BJ, Liu CM,  
849 Hayer M, McHugh TA *et al*: **Phylogenetic organization of bacterial activity.** *ISME Journal*  
850 2016, **10(9):2336-2340.**
- 851 58. Caporaso JG, Lauber CL, Walters WA, Berg-Lyons D, Lozupone CA, Turnbaugh PJ, Fierer N,  
852 Knight R: **Global patterns of 16S rRNA diversity at a depth of millions of sequences per**  
853 **sample.** *PNAS* 2011, **108:4516-4522.**

- 854 59. Hugerth LW, Wefer HA, Lundin S, Jakobsson HE, Lindberg M, Rodin S, Engstrand L,  
855 Andersson AF: **DegePrime, a program for degenerate primer design for broad-taxonomic-**  
856 **range PCR in microbial ecology studies.** *ISME Journal* 2014, **5**(10):1571-1579.
- 857 60. Edgar RC: **UNOISE2: improved error-correction for Illumina 16S and ITS amplicon**  
858 **sequences.** *bioRxiv* 2016:<http://dx.doi.org/10.1101/081257>.
- 859 61. Edgar RC: **UPARSE: highly accurate OTU sequences from microbial amplicon reads.** *Nature*  
860 *Methods* 2013, **10**(10):996-998.
- 861 62. McKinney W: **Data Structures for Statistical Computing in Python.** *Proceedings of the 9th*  
862 *Python in Science Conference* 2010, **51-56**.
- 863 63. Oliphant TE: **A guide to NumPy.** USA: Trelgol Publishing; 2006.
- 864 64. Hunter JD: **Matplotlib: A 2D Graphics Environment.** *Computing in Science & Engineering*  
865 2007, **9**:90-95.
- 866 65. Mantel N: **The detection of disease clustering and a generalized regression approach.**  
867 *Cancer Research* 1967, **27**(2 Part 1):209-220.
- 868 66. Anderson MJ: **A new method for non-parametric multivariate analysis of variance.** *Austral*  
869 *Ecol* 2001, **26**(1):32-46.
- 870 67. Virtanen P, Gommers R, Oliphant TE, Haberland M, Reddy T, Cournapeau D, Burovski E,  
871 Peterson P, Weckesser W, Bright J *et al*: **SciPy 1.0--Fundamental Algorithms for Scientific**  
872 **Computing in Python.** *arXiv:190710121* 2019.